JACS
JOURNAL OF THE AMERICAN CHEMICAL SOCIETY
Article
pubs.acs.org/JACS

Ion-Based Materials Derived from Positively and Negatively Charged Chloride Complexes of π-Conjugated Molecules

Bin Dong,[†,∞] Tsuneaki Sakurai,[‡] Yuya Bando,[†] Shu Seki,*[,‡] Kazuto Takaishi,[§,∥] Masanobu Uchiyama,[§,⊥] Atsuya Muranaka,[§,#] and Hiromitsu Maeda*[,†]

[†]College of Pharmaceutical Sciences, Ritsumeikan University, Kusatsu 525-8577, Japan
[‡]Department of Applied Chemistry, Graduate School of Engineering, Osaka University, Suita 565-0871, Japan
[§]Advanced Elements Chemistry Research Team and Elements Chemistry Laboratory, RIKEN, Wako 351-0198, Japan
[∥]Faculty of Science and Technology, Seikei University, Musashino 180-8633, Japan
[⊥]Graduate School of Pharmaceutical Sciences, The University of Tokyo, Tokyo 113-0033, Japan
[#]PRESTO, Japan Science and Technology Agency (JST), Kawaguchi 332-0012, Japan

Supporting Information

ABSTRACT: Oriented salts from planar charged species were prepared by combining positively and negatively charged receptor−anion complexes with similar geometries using dicationic and electronically neutral π-conjugated receptors. Phenylene- or pyrimidine-bridged bis(imidazolium) dicationic anion receptors formed monocationic receptor−Cl^- complexes that were accompanied by a free Cl^-. This free Cl^- was subsequently captured by pyrrole-based neutral anion receptors to form negatively charged receptor−Cl^- complexes. The ion pair of the resulting positively and negatively charged planar receptor−Cl^- complexes could produce a supramolecular octane gel, adopting a lamellar self-organized structure in its xerogel state. On the other hand, the solid-state ion pairs had hexagonal columnar mesophases, which formed via alternate stacking of the positively and negatively charged planar receptor−Cl^- complexes. By use of the flash-photolysis time-resolved microwave conductivity technique, the one-dimensional charge-carrier transporting property, with a mobility of 0.05 $cm^2\ V^{-1}\ s^{-1}$, was determined for the newly prepared solid-state ion pairs.

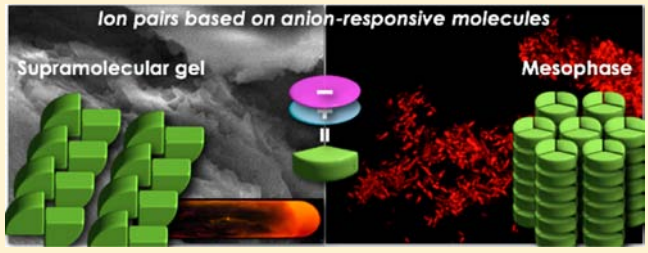

INTRODUCTION

An effective strategy to prepare useful materials involves appropriate arrangement of electronically functional ionic organic species.[1,2] In particular, segregated stacking of cations and anions in assemblies[3] can provide potential organic semiconductive materials. One expected advantage of such charge-based assemblies is high carrier density because of weaker electrostatic repulsions between identical charged species by increasing the number of electronically neutral charge carriers. This is in contrast to the properties of materials composed of electronically neutral components that exhibited electrostatic repulsion between their ionic carriers. Promising candidates for the negatively charged components are anion complexes of appropriate electronically neutral receptor molecules.[4,5] Among them, pyrrole-based π-conjugated molecules (e.g., **1a**−**c**, Figure 1a)[6] form receptor−anion complexes as planar anionic structures, which afford a variety of ion-based assemblies for use as soft materials by combining with suitable counter cations.[7−9] A promising cation as a building subunit is a planar triazatriangulenium ($TATA^+$) cation,[10] which can form the organized structures from the partial contributions of charge-segregated assemblies and charge-by-charge assemblies of alternately stacking cations and anions.[8a] Combination of $TATA^+$ and receptor−anion complexes results in the ion-based thermotropic liquid crystals that exhibit an ambipolar electrical conductivity.[9] However, the formation of functional ion-based assemblies requires design and preparation of more suitable cationic species. In this study, dicationic anion receptors[11] are focused on because such receptors could afford monocationic receptor−anion complexes by binding a single anion. The objective of this study is to report the formation of ion pairs and to determine the assembling behavior of positively and negatively charged receptor−anion complexes. For example, bis(imidazolium)-substituted molecules, acting as dicationic π-conjugated anion receptors, can form a [1 + 1]-type anion complex accompanied by a free anion,[12] which is a component of ion pairs with pyrrole-based anion receptors **1a**−**c**. Therefore, phenylene- and pyrimidine-linked bis(imidazolium) dications ($\mathbf{2a}^{2+}$ and $\mathbf{3a}^{2+}$/$\mathbf{3b}^{2+}$, respectively, Figure 1b) were selected as dicationic anion receptors for this study.[13]

Received: July 12, 2013
Revised: September 4, 2013
Published: September 5, 2013

   dx.doi.org/10.1021/ja4071333 | J. Am. Chem. Soc. 2013, 135, 14797−14805

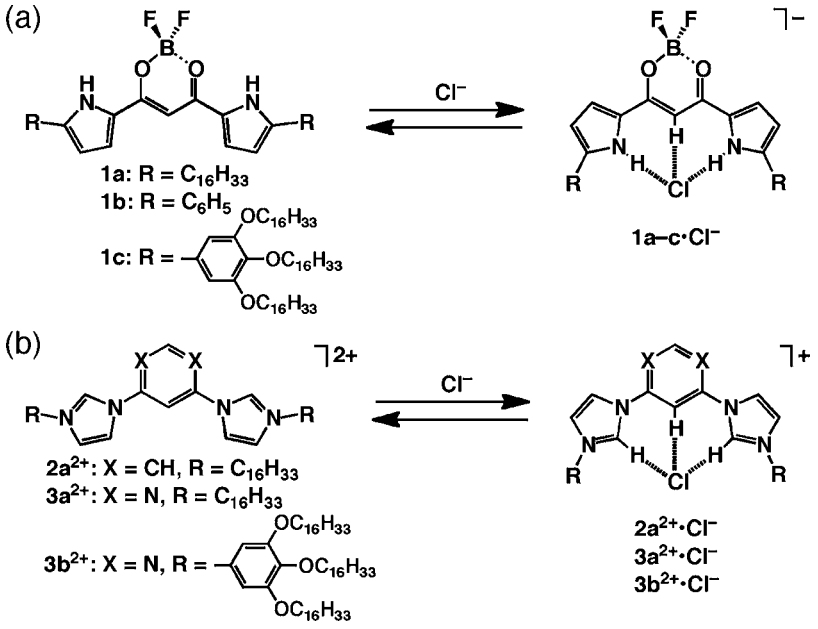

Figure 1. (a) Electronically neutral anion receptors **1a**–**c** and (b) positively charged anion receptors $\mathbf{2a}^{2+}$, $\mathbf{3a}^{2+}$, and $\mathbf{3b}^{2+}$ in their Cl^--binding modes form anionic and cationic receptor–Cl^- complexes, respectively.

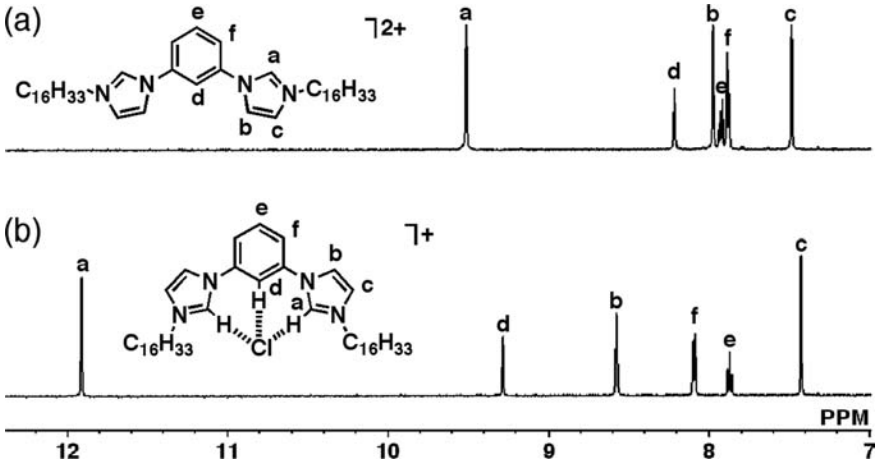

Figure 2. Partial ^1H NMR spectra of (a) $\mathbf{2a}^{2+}\cdot 2BF_4^-$ and (b) $\mathbf{2a}^{2+}\cdot 2Cl^-$ (1.0×10^{-3} M) in CD_2Cl_2 at 20 °C.

RESULTS AND DISCUSSION

Bis(imidazolium)benzene dichloride $\mathbf{2a}^{2+}\cdot 2Cl^-$ was synthesized by alkylation of bis(imidazolyl)benzene with *n*-chloroalkane,[13b] and bis(imidazolium)pyrimidine dichloride $\mathbf{3a}^{2+}\cdot 2Cl^-$ and $\mathbf{3b}^{2+}\cdot 2Cl^-$ were obtained by the reaction of 4,6-dichloropyrimidine with the corresponding imidazole derivatives.[13a] By use of anion exchange with $LiBF_4$, $\mathbf{2a}^{2+}$ and $\mathbf{3a}^{2+}$ as tetrafluoroborate (BF_4^-) salts were prepared to test their anion-binding properties. For example, the change of the counteranion from BF_4^- to Cl^- for $\mathbf{2a}^{2+}$ resulted in ^1H NMR spectral changes, namely, the downfield shifts of imidazole CH^a and benzene CH^d from 9.51 and 8.21 ppm to 11.91 and 9.28 ppm, respectively (Figure 2). This observation suggested that the two groups act as Cl^--binding sites. The moderate downfield shifts of imidazole CH^b and benzene CH^f from 7.97 and 7.93 ppm to 8.58 and 8.10 ppm, respectively, implied changes in the magnetic environment upon tight interaction with Cl^-. The Cl^--binding behavior was further confirmed by the absence and presence of ^1H–^1H NOESY cross peaks between CH^a and CH^d for BF_4^- and Cl^- salts, respectively. The binding constant values (K_a) for $\mathbf{2a}^{2+}$ and $\mathbf{3a}^{2+}$ with Cl^- were 130 000 and 250 000 M^{-1}, respectively, which were estimated using a 1:1 curve fitting of the changes in the UV/vis absorption upon addition of a tetrabutylammonium (TBA^+) salt into the CH_2Cl_2 solutions of the BF_4^- salts. The stronger anion-binding affinity of $\mathbf{3a}^{2+}$ compared to $\mathbf{2a}^{2+}$ is caused by the fact that the pyrimidine ring is more electronically deficient than the benzene ring and also because the optimized structure of the $\mathbf{3a}^{2+}$ skeleton has a higher planarity than the optimized structure of the $\mathbf{2a}^{2+}$ skeleton.[14] Electrostatic interactions that support hydrogen bonding resulted in a higher K_a for the positively charged anion receptors, considering the K_a values of **1a** (4000 M^{-1})[6b] and **1b** (30 000 M^{-1})[6a] for Cl^- as a TBA salt in CH_2Cl_2.

Theoretical calculations at the B3LYP/6-31G(d,p) level using the SCRF-PCM method were carried out to predict the ion-pair formation of positively and negatively charged receptor–anion complexes in CH_2Cl_2.[14] The dicationic receptors $\mathbf{2a}'$ and $\mathbf{3a}'$ with methyl substituents in place of **2a**

dx.doi.org/10.1021/ja4071333 | J. Am. Chem. Soc. 2013, 135, 14797–14805

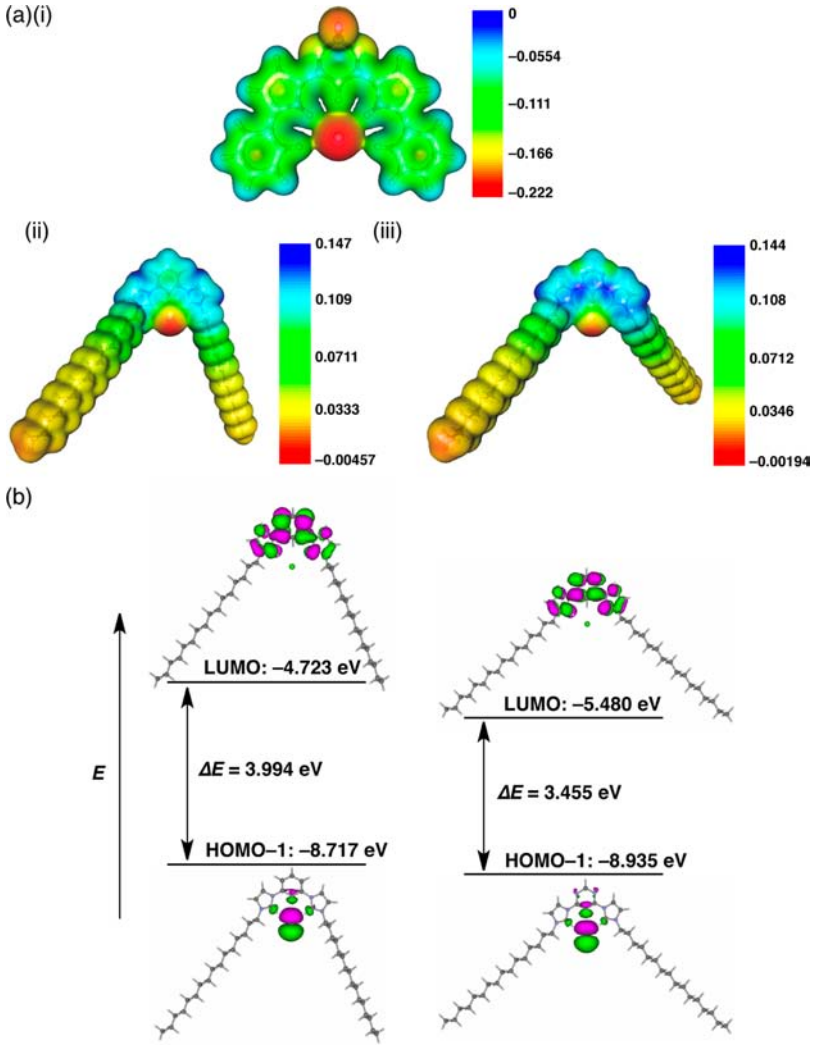

Figure 3. (a) Electrostatic potentials mapped onto the electron density isosurfaces (δ = 0.001) of (i) **1b**·Cl^-,[9a] (ii) $\mathbf{2a}^{2+}$·Cl^-, and (iii) $\mathbf{3a}^{2+}$·Cl^- and (b) molecular orbitals (HOMO−1 and LUMO) of $\mathbf{2a}^{2+}$·Cl^- (left) and $\mathbf{3a}^{2+}$·Cl^- (right) by single-point calculations at B3LYP/6-31+G(d,p) based on the optimized structures at B3LYP/6-31G(d,p). In (b), the HOMO orbitals located at Cl^- are omitted.

and **3a**, respectively, were used as model compounds. The sums of the energy values for positively and negatively charged receptor−anion complexes ($\mathbf{2a'}^{2+}$·Cl^- + **1b**·Cl^- and $\mathbf{3a'}^{2+}$·Cl^- + **1b**·Cl^-) as ion pairs are smaller by 4.44 and 6.95 kcal mol^{-1}, respectively, than those for the starting materials ($\mathbf{2a'}^{2+}$·$2Cl^-$ + **1b** and $\mathbf{3a'}^{2+}$·$2Cl^-$ + **1b**), suggesting that formation of these planar charged species is plausible in solution and bulk states. In the starting state, ion pairs $\mathbf{2a'}^{2+}$·$2Cl^-$ and $\mathbf{3a'}^{2+}$·$2Cl^-$ exist as [1 + 1]-type complexes $\mathbf{2a'}^{2+}$·Cl^- and $\mathbf{3a'}^{2+}$·Cl^- accompanied by a weakly associated Cl^-. On the basis of the theoretical study, one of the two Cl^- anions with the dicationic species **2a′** and **3a′** is better to be captured by another anion receptor such as **1b**. The stabilization owing to the Cl^- binding by **1b** is more effective in **3a′** than **2a′** possibly because of the weaker interaction in **3a′** for a relatively free Cl^- as the starting state. Furthermore, electrostatic potential mapping diagrams of the cationic receptor−anion complexes $\mathbf{2a}^{2+}$·$Cl^-$and $\mathbf{3a}^{2+}$·Cl^- along with the anionic complex **1b**·Cl^-, in place of **1c**·Cl^- for facile calculation, were estimated at B3LYP/6-31+G(d,p)//B3LYP/6-31G(d,p) (Figure 3a). As shown in these diagrams, negative charges of the bound Cl^- anions are more highly delocalized in dicationic $\mathbf{2a}^{2+}$ and $\mathbf{3a}^{2+}$ than electronically neutral **1b**. Among the cationic complexes, $\mathbf{3a}^{2+}$·Cl^- showed more electron-deficient property than $\mathbf{2a}^{2+}$·Cl^- because of the pyrimidine nitrogen units, as also shown in the lower HOMO−1 and LUMO of $\mathbf{3a}^{2+}$·Cl^- than those of $\mathbf{2a}^{2+}$·Cl^- (Figure 3b). We can expect the formation of stacking ion pairs from the cationic and anionic receptor−anion complexes, although it is not easy to predict their possible stacking modes based on the theoretical study.

Since it is difficult to estimate the ion-pairing behavior of positively and negatively charged Cl^- complexes in CH_2Cl_2, assemblies based on ion-pairing in a less polar solvent were examined. In fact, the complex of **1c** (10 mg mL^{-1}) and $\mathbf{3a}^{2+}$·$2Cl^-$ with a 1:1 molar ratio in octane formed a supramolecular gel with a solution−gel transition temperature ($T_{sol-gel}$) of 6 °C (Figure 4a). This gel state of the ion pairs of Cl^- complexes obviously differed from the solution state for the Cl^- complex of **1c** as a TBA salt in octane, although the $T_{sol-gel}$ value was lower than that (27 °C) of **1c** without Cl^- binding.[6a] This observation could be ascribed to the difference in the geometries of cationic species: fairly planar $\mathbf{3a}^{2+}$·Cl^- and bulky TBA^+. Assembly in the gel state was also observed in UV/vis absorption and fluorescence spectra, although the detailed discussion of the molecular orientations was challenging because of the system comprising multiple π-

dx.doi.org/10.1021/ja4071333 | J. Am. Chem. Soc. 2013, 135, 14797−14805

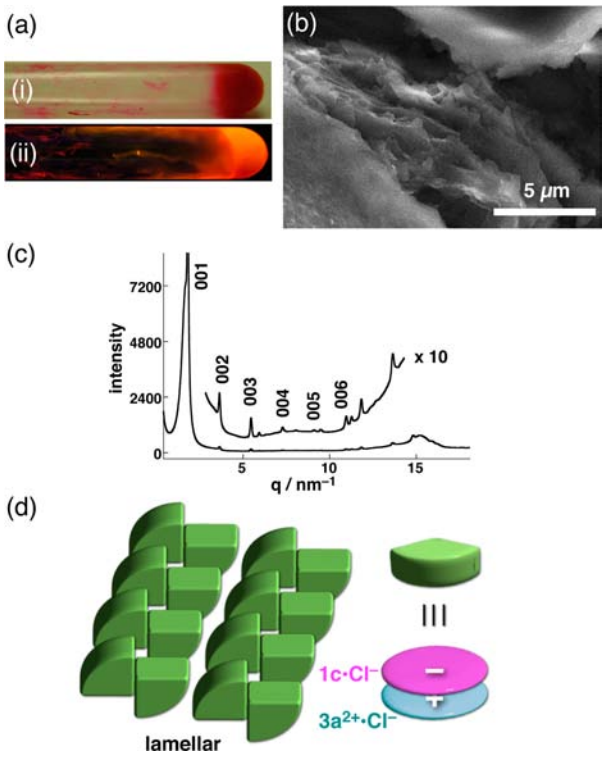

Figure 4. (a) Photos of gel at 6 °C under (i) visible light and (ii) UV_{365nm} light of the complex of **1c** (10 mg mL^{-1}) and $\mathbf{3a}^{2+}\cdot 2Cl^-$ in a 1:1 molar ratio in octane, (b) SEM image on silicon substrate, (c) XRD pattern, and (d) the proposed lamellar model, wherein exact molecular orientation cannot be shown, of the xerogel of $\mathbf{1c}\cdot Cl^-\mathbf{-3a}^{2+}\cdot Cl^-$ after freeze-drying.

electronic components with less symmetrical geometries. In the long-wavelength region, the gel had broad UV/vis absorption bands with two maxima at 519 and 538 nm, in contrast to that of the solution state that had a maximum at 525 nm. The red shift reflected the formation of stacking structures in the gel state. The fluorescence emission maximum of the gel appeared at 583 nm, with a shoulder at 623 nm, when excited at 538 nm. These peaks were also red-shifted compared to the solution state (λ_{em} = 577 nm, excited at 525 nm). Under scanning electron microscopy (SEM), sheetlike structures were observed at a cracked edge of the xerogel on silicon after freeze-drying (Figure 4b). The xerogel was further measured by synchrotron X-ray diffraction (XRD), with *d*-spacings of 3.47, 1.73, 1.15, 0.86, 0.69, and 0.57 nm corresponding to (001), (002), (003), (004), (005), and (006), respectively (Figure 4c). The XRD data indicated the formation of a lamellar structure consisting of the positively and negatively charged planar receptor−Cl^- complexes $\mathbf{3a}^{2+}\cdot Cl^-$ and $\mathbf{1c}\cdot Cl^-$, respectively (Figure 4d). The sheetlike morphology observed by SEM can be correlated with the formation of lamellar structures. Although the noncovalent interactions between $\mathbf{3a}^{2+}\cdot Cl^-$ and $\mathbf{1c}\cdot Cl^-$ may not be as strong as the interactions between **1c**, they can retain the gel state at lower temperatures. On the other hand, because of the poor solubility of $\mathbf{2a}^{2+}\cdot 2Cl^-$ and $\mathbf{3b}^{2+}\cdot 2Cl^-$, the mixture of **1c** and $\mathbf{2a}^{2+}\cdot 2Cl^-$ with **1c** and $\mathbf{3b}^{2+}\cdot 2Cl^-$ did not totally dissolve in octane after heating and sonication.

The solid-state ion-pairing materials of positively and negatively charged receptor−Cl^- complexes were prepared by slowly evaporating the CH_2Cl_2 solutions in equivalent molar ratios of **1b**,**c** and dicationic receptors as Cl^- salts ($\mathbf{2a}^{2+}\cdot 2Cl^-$ and $\mathbf{3a}^{2+}/\mathbf{3b}^{2+}\cdot 2Cl^-$), whose compositions were confirmed by ^1H NMR spectroscopy and elemental analysis. Both **1b**- and **1c**-based ion pairs were red solids with absorption maxima around 540 nm at room temperature after melting, and their emission maxima were around 585 and 600 nm, respectively. The thermal behaviors of the solid-state ion pairs were examined using polarizing optical microscopy (POM) and differential scanning calorimetry (DSC). In the POM measurements, typical textures such as broken-fan-shaped types were observed during heating and cooling processes (Figure 5a for $\mathbf{1c}\cdot Cl^-\mathbf{-3a}^{2+}\cdot Cl^-$), indicating the formation of mesophases. The phase transitions of the ion pairs with a fixed neutral anion receptor (**1b** or **1c**) varied based on the linkage spacers and the substituents on the imidazole ring in the dicationic anion receptors. No transition peaks appeared in the DSC thermograms of the ion pairs with $\mathbf{1b}\cdot Cl^-$, although some birefringent textures were observed with POM. On the other hand, the phase transition temperatures (°C) of the ion pairs with $\mathbf{1c}\cdot Cl^-$ were detected by DSC (5 °C min^{-1}) as 103.9/46.7 ($\mathbf{1c}\cdot Cl^-\mathbf{-2a}^{2+}\cdot Cl^-$), 148.3/33.9 ($\mathbf{1c}\cdot Cl^-\mathbf{-3a}^{2+}\cdot Cl^-$), and 119.3/28.8 ($\mathbf{1c}\cdot Cl^-\mathbf{-3b}^{2+}\cdot Cl^-$) upon cooling from an isotropic liquid state (Iso) (part i of Figure 5b). These observations were significantly different from those of the individual components; **1c** showed a mesophase at 36.7−172.5 °C,[6c] whereas $\mathbf{2a}^{2+}\cdot 2Cl^-$, $\mathbf{3a}^{2+}\cdot 2Cl^-$, and $\mathbf{3b}^{2+}\cdot 2Cl^-$ exhibited phase transitions at 213.5 (from POM)/84.3, 155.9/23.5, and 158.2/45.0 °C, respectively, upon cooling from Iso (part ii of Figure 5b). The temperature range of the mesophase in $\mathbf{1c}\cdot Cl^-\mathbf{-3a}^{2+}\cdot Cl^-$ is greater than that in $\mathbf{1c}\cdot Cl^-\mathbf{-2a}^{2+}\cdot Cl^-$ by incorporation of pyrimidine moieties. In addition, introduction of the aryl rings possessing three aliphatic chains in $\mathbf{1c}\cdot Cl^-\mathbf{-3b}^{2+}\cdot Cl^-$ makes a smaller mesophase temperature range compared to $\mathbf{1c}\cdot Cl^-\mathbf{-3a}^{2+}\cdot Cl^-$, suggesting that the dicationic π-conjugated species can control the properties of ion-pair-based assemblies.

The detailed structures in each phase were assigned using synchrotron XRD measurements. The XRD pattern of $\mathbf{1c}\cdot Cl^-\mathbf{-3a}^{2+}\cdot Cl^-$ in the mesophase at 115 °C had *d*-spacings of 3.76, 2.17, 1.50, and 1.26 nm which correspond to (100), (110), (210), and (300), respectively (part i of Figure 5c), indicating a hexagonal columnar (Col_h) structure with a lattice parameter of a = 4.34 nm. Besides these sharp in-plane diffractions, a broad and weak peak appeared around 0.75 nm, which was derived from the stacking periodicity (c) between the adjacent assembled units. After cooling to 20 °C, the Col_h structure was maintained with peaks at 4.09, 2.40, 1.97, and 1.60 nm indexed as (100), (110), (200), and (210), respectively, giving a = 4.73 nm, and the peak at 0.75 nm became more evident (part ii of Figure 5c). The smaller a value at higher temperatures was caused by a greater degree of melting of the alkyl chains. Accordingly, the average number of ion pairs in an assembled unit (Z) was estimated to be 3 for ρ = 1 (Z = 2.9 at 115 °C and Z = 3.4 at 20 °C). The c values were similar to those of the charge-by-charge assemblies previously observed in the crystal of $\mathbf{1b}\cdot Cl^-$−$TATA^+$ and in the mesophase of $\mathbf{1c}\cdot Cl^-$−$TATA^+$.[8a] Thus, we concluded that the alternately stacking positively and negatively charged planar receptor−Cl^- complexes ($\mathbf{3a}^{2+}\cdot Cl^-$ and $\mathbf{1c}\cdot Cl^-$, respectively) afforded charge-by-charge-based Col_h structures (Figure 5d). This contrasts with the observed lamellar structure in the xerogel, which suggested that the more ordered structures were constructed by thermal annealing. Meanwhile, $\mathbf{1c}\cdot Cl^-\mathbf{-2a}^{2+}\cdot Cl^-$ also provided a Col_h structure (a = 4.65 nm, c = 0.75 nm, Z = 3.3 for ρ = 1 at 80 °C upon cooling from Iso), whereas $\mathbf{1c}\cdot Cl^-\mathbf{-3b}^{2+}\cdot Cl^-$ had

dx.doi.org/10.1021/ja4071333 | J. Am. Chem. Soc. 2013, 135, 14797−14805

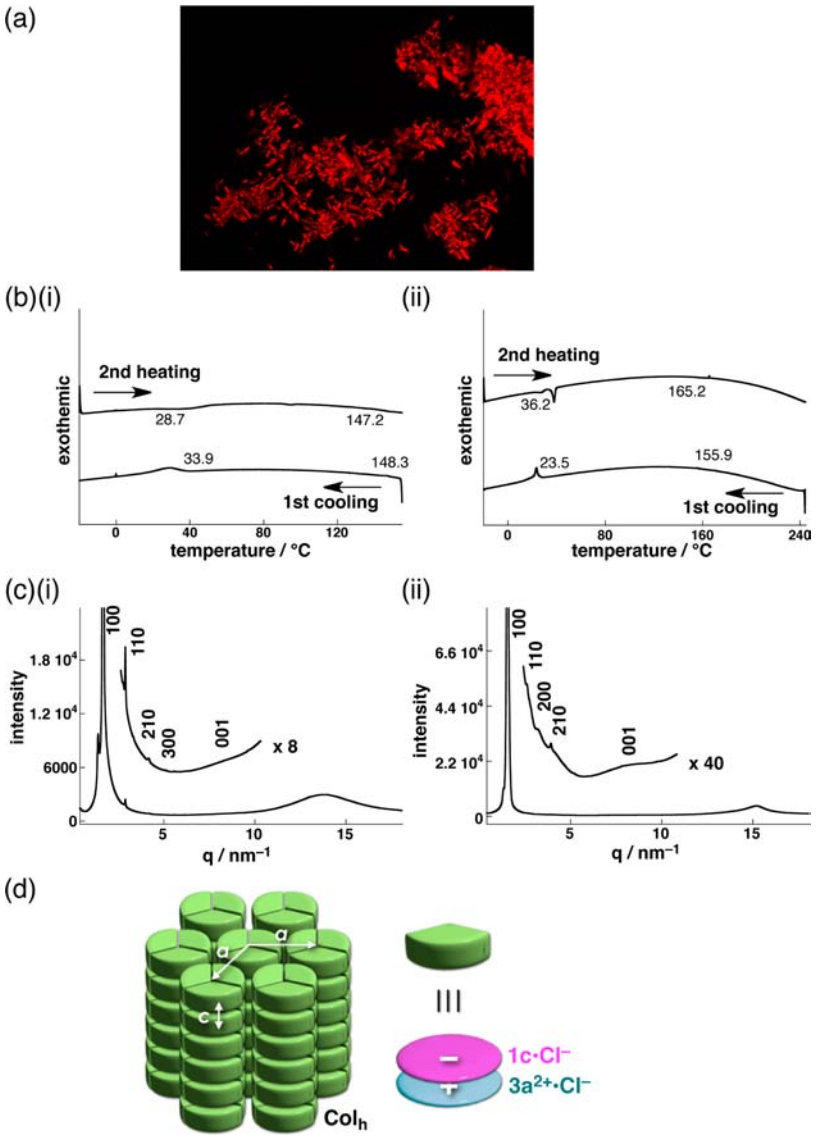

Figure 5. (a) POM texture of **1c**·Cl^-−**3a**$^{2+}$·Cl^- at 115 °C, (b) DSC thermograms (5 °C/min) of (i) **1c**·Cl^-−**3a**$^{2+}$·Cl^- and (ii) **3a**$^{2+}$·2Cl^-, wherein onset temperatures (°C) of phase transitions are labeled although some peaks are weak, (c) XRD patterns at (i) 115 °C and (ii) 20 °C upon cooling from Iso, and (d) a proposed Col_h model of **1c**·Cl^-−**3a**$^{2+}$·Cl^-, wherein exact molecular orientation cannot be shown.

complicated XRD patterns, which may be ascribed to the increased rigidity of the dicationic anion receptor with introduction of aryl moieties. These assembled structures are quite different from the individual components **1c** (Col_h with the parameters of a = 3.98 nm, c = 0.45 nm, $Z \approx 2$ for ρ = 1 at 170 °C),[6c] **2a**$^{2+}$·2Cl^- (lamellar with the thickness of 3.72 nm at 160 °C), **3a**$^{2+}$·2Cl^- (lamellar with the thickness of 3.85 nm at 115 °C), and **3b**$^{2+}$·2Cl^- (Col_h with the parameters of a = 4.57 nm, c = 0.38 nm, $Z \approx 2$ for ρ = 1 at 90 °C), whose data were obtained upon cooling from Iso. The observations by synchrotron XRD indicated that the introduction of dicationic anion receptors as precursors of planar cations was effective to construct ordered assembled structures. It is noteworthy that the geometries in the core π-conjugated parts of the cationic and anionic receptor−Cl^- complexes are quite similar by considering the constituents, one six-membered ring at the center and two neighboring five-membered rings. The similarity in the sizes and shapes of two ionic components is a very important factor to form assemblies consisting of multiple components.

To investigate the charge-carrier transporting property of the one-dimensionally arranged planar cation−anion systems, we carried out flash-photolysis time-resolved microwave conductivity (FP-TRMC) measurements for **1c**·Cl^-−**2a**$^{2+}$·Cl^- and **1c**·Cl^-−**3a**$^{2+}$·Cl^-. As previously reported,[15] the FP-TRMC method is concerned with the local motion of the photochemically generated charge carrier species. Upon photoexcitation with a 355 nm laser pulse, both **1c**·Cl^-−**2a**$^{2+}$·Cl^- and **1c**·Cl^-−**3a**$^{2+}$·Cl^- on a quartz plate displayed a typical rise−decay profile of conductivity ($\phi\sum\mu$), where ϕ and $\sum\mu$ denote the quantum yield of charge-carrier generation and sum of the charge-carrier mobilities, respectively. Taking into account the principle of the FP-TRMC technique, the observed long lifetimes of the charge carriers indicate that their transport events take place along the columnar axis during the measurements. We also found that the maximum values of the signal $(\phi\sum\mu)_{max}$ were approximately 1.2×10^{-5} and 1.0×10^{-5} cm^2 V^{-1} s^{-1} for **1c**·Cl^-−**2a**$^{2+}$·Cl^- and **1c**·Cl^-−**3a**$^{2+}$·Cl^-, respectively (Figure 6). Estimation of ϕ values from the direct current method using comb-type interdigitated electrodes on a glass substrate[15c] finally allowed

dx.doi.org/10.1021/ja4071333 | J. Am. Chem. Soc. 2013, 135, 14797−14805

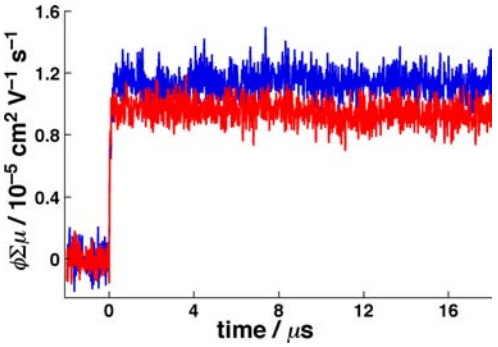

Figure 6. TRMC profiles of **1c**·Cl^-−**2a**$^{2+}$·Cl^- (blue line) and **1c**·Cl^-−**3a**$^{2+}$·Cl^- (red line) upon excitation at 355 nm.

for estimation of intrinsic charge-carrier mobilities $\sum\mu$ of 0.05 and 0.03 cm^2 V^{-1} s^{-1} for **1c**·Cl^-−**2a**$^{2+}$·Cl^- and **1c**·Cl^-−**3a**$^{2+}$·Cl^-, respectively. This suggests that the stacking of **1c** in the columnar manner provides effective hopping transport pathways for positive charges with a small contribution of charge localization and hopping barrier enhancement by the counter Cl^-. In addition, as described in the previous paragraph, the similar geometries of the cationic and anionic receptor−Cl^- complexes should be effective for constructing the conductive pathways. The observed difference in the charge carrier mobility between **1c**·Cl^-−**2a**$^{2+}$·Cl^- and **1c**·Cl^-−**3a**$^{2+}$·Cl^- proposes the tunability on the electronic performance by choosing the receptor molecules. In fact, **1c**·Cl^-−**2a**$^{2+}$·Cl^- in XRD showed the slightly smaller stacking periodicity than **1c**·Cl^-−**3a**$^{2+}$·Cl^- at room temperature, which might be the reason for higher mobility for **1c**·Cl^-−**2a**$^{2+}$·Cl^-. Another reason may be the less electron-deficient **2a**$^{2+}$·Cl^- than **3a**$^{2+}$·Cl^- (Figure 3) as a building unit of charge-by-charge-based columnar structures with **1c**·Cl^-. This also suggests obviously a crucial role of cationic anion receptors in the design of the present materials system for optimization of electron mobility via LUMO.

SUMMARY

Two anions accompanied by dicationic anion receptors were bound by dicationic and neutral anion receptors to yield positively and negatively charged receptor−anion complexes, respectively, with similar geometries and consequently provided ion-pairing materials. The positively and negatively charged planar receptor−anion complexes formed lamellar structures in the gel state. However, the planar ion pairs interacted more efficiently and produced more ordered Col_h mesophases with charge-by-charge structures upon thermal annealing. Although it is not easy to synthesize planar ions, especially planar anions, this study reveals a feasible noncovalent approach of synthesizing planar cations and anions in one system. A notable feature in this study is the formation of positively and negatively charged species as the complexes with identical ionic species (Cl^-). Charge control of π-conjugated molecules by Cl^- binding is a key strategy to form dimension-controlled organized structures. A similar strategy to fabricate ordered structures comprising oppositely charged components can also be applied to complexes with metal ions as observed in Magnus salt.[16] Furthermore, considering the observed charge-carrier transporting property of the resulting ion-pairing materials in FP-TRMC and the tunability of receptor molecules to change the conductivity values, we believe that suitable design and preparation of cationic or neutral anion receptors further develop a variety of advanced planar-charge-based materials for targeted applications.

EXPERIMENTAL SECTION

General Procedures. Starting materials were purchased from Wako Pure Chemical Industries Ltd., TCI Chemical Co., and Sigma-Aldrich Co., which were used without further purification. BF_2 complexes **1b,c** were synthesized according to the literature.[6a] ^1H NMR spectra were recorded on a JEOL ECA-600 600 MHz spectrometer and were referenced to solvent. Electrospray ionization time-of-flight mass spectrometric studies (ESI-TOF-MS) were conducted using a Bruker microTOF focus instrument in the positive and negative ion modes. UV/vis absorption and fluorescence spectra were recorded on Hitachi U-3500 and F-4500 spectrometers for solutions, respectively. Solid-state UV/vis absorption and fluorescence spectra were recorded on a System Instruments surface and interface spectrometer SIS-50 and a Hamamatsu quantum yields measurements system for organic LED materials C9920-02, respectively. Elemental analyses were performed on a Yanaco CHN corder MT series for carbon, hydrogen, and nitrogen and with the oxygen flask combustion method and the subsequent potentiometric titration of silver using sodium ion selective glass electrode, wherein the data were recorded on a Hiranuma Sangyo Co. Ltd. autotitrator RAT-IIS for chlorine at the Laboratory for Organic Elemental Microanalysis, Kyoto University. Column chromatography was performed on Wakogel C-300.

1,3-Bis(3-hexadecylimidazolium)benzene Dichloride, 2a^{2+}·2Cl^-. 2a^{2+}·2Cl^- was synthesized by the reaction of imidazole with 1,3-dibromobenzene followed by the alkylation of bis(imidazolyl)benzene with 1-chlorohexadecane.[13b] In a two-necked round-bottom flask (50 mL) equipped with a reflux condenser and a magnetic stirrer, bis(imidazolyl)benzene (0.7 mmol) was dissolved in DMF (5 mL) and 1-chlorohexdecane (3.5 mmol) was added under nitrogen. The mixture was stirred at 140 °C for 48 h, cooled, and the precipitate was isolated by filtration and then recrystallized from CH_2Cl_2/*n*-hexane to give 2a^{2+}·2Cl^-. Yield: 37%. ^1H NMR (600 MHz, CD_2Cl_2, 20 °C): δ (ppm) 11.91 (s, 2H, imidazole-H), 9.28 (s, 1H, Ar-H), 8.58 (s, 2H, imidazole-H), 8.10 (d, J = 7.8 Hz, 2H, Ar-H), 7.87 (t, J = 7.8 Hz, 1H, Ar-H), 7.42 (s, 2H, imidazole-H), 4.39 (t, J = 7.2 Hz, 4H, NCH_2), 2.07−2.02 (m, 4H, NCH_2CH_2), 1.44−1.22 (m, 52H, $NC_2H_4(CH_2)_{13}$), 0.87 (t, J = 7.2 Hz, 6H, $NC_{15}H_{30}CH_3$). ^{13}C NMR (151 MHz, $CDCl_3$, 20 °C): δ (ppm) 136.38, 135.96, 132.72, 122.71, 122.59, 122.20, 114.58, 50.83, 32.01, 30.24, 29.77, 29.74, 29.69, 29.61, 29.48, 29.44, 29.10, 26.41, 22.77, 14.19 (some of the signals for hexadecyl chains were overlapped). ESI-TOF-MS (positive, % intensity): m/z 330.3 (32), 330.8 (15), 695.6 (100), 696.6 (47). Calcd for $C_{44}H_{76}N_4^{2+}$ ([M − 2Cl]$^{2+}$), 660.61; $C_{44}H_{76}N_4Cl^+$ ([M − Cl]$^+$), 695.68. ESI-TOF-MS (negative, % intensity): m/z 765.5 (100), 766.5 (46). Calcd for $C_{44}H_{76}Cl_3N_4^-$ ([M + Cl]$^-$): 765.51. Elemental analysis: calcd (%) for $C_{44}H_{76}Cl_2N_4·H_2O$, C 70.46, H 10.48, Cl 9.45, N 7.47, O 2.13; found C 70.18, H 10.68, Cl 9.41, N 7.42.

1,3-Bis(3-hexadecylimidazolium)benzene Tetrafluoroborate, 2a^{2+}·2BF_4^-. 2a^{2+}·2BF_4^- was prepared by the ion exchange of 2a^{2+}·2Cl^-. 2a^{2+}·2Cl^- (0.22 mmol) was dissolved in CH_2Cl_2 (4 mL) and added to a solution of $LiBF_4$ (0.46 mmol) dissolved in water (2 mL) in a glass bottle. The mixture was stirred over 10 min until no further precipitate appeared. The precipitate was isolated by filtration and washed with EtOAc. Yield: 75%. ^1H NMR (600 MHz, CD_2Cl_2, 20 °C): δ (ppm) 9.51 (s, 2H, imidazole-H), 8.21 (s, 1H, Ar-H), 7.97 (s, 2H, imidazole-H), 7.93 (t, J = 7.8 Hz, 1H, Ar-H), 7.88 (d, J = 7.8 Hz, 2H, Ar-H), 7.48 (s, 2H, imidazole-H), 4.34 (t, J = 7.2 Hz, 4H, NCH_2), 2.01−1.97 (m, 4H, NCH_2CH_2), 1.43−1.19 (m, 52H, $NC_2H_4(CH_2)_{13}$), 0.87 (t, J = 7.2 Hz, 6H, $NC_{15}H_{30}CH_3$). ^{13}C NMR (151 MHz, $CDCl_3$, 20 °C): δ (ppm) 135.95, 134.83, 132.76, 123.47, 123.35, 121.77, 115.83, 50.95, 32.06, 30.01, 29.86, 29.80, 29.75, 29.60, 29.49, 29.16, 26.47, 22.81, 14.19 (some of the signals for hexadecyl chains were overlapped). ESI-TOF-MS (positive, % intensity): m/z 330.3 (91), 330.8 (41), 747.6 (100), 748.6 (42). Calcd for $C_{44}H_{76}N_4^{2+}$ ([M − 2BF_4]$^{2+}$), 660.61; $C_{44}H_{76}N_4BF_4^+$ ([M − BF_4]$^+$), 747.61. ESI-TOF-MS

dx.doi.org/10.1021/ja4071333 | J. Am. Chem. Soc. 2013, 135, 14797−14805

(negative, % intensity): m/z 86.0 (19), 87.0 (100). Calcd for BF_4^- ($[0.5M - 0.5C_{44}H_{76}N_4]^-$): 87.00. Elemental analysis: calcd (%) for $C_{44}H_{76}B_2F_8N_4$, C 63.31, H 9.18, B 2.59, F 18.21, N 6.71; found C 63.04, H 9.44, N 6.75 (for the species containing B, the exact value of F cannot be estimated).

4,6-Bis(3-hexadecylimidazolium)pyrimidine Dichloride, $3a^{2+}\cdot 2Cl^-$. $3a^{2+}\cdot 2Cl^-$ was obtained by the reaction of 1-hexadecylimidazole[17] with 4,6-dichloropyrimidine.[13a] In a two-necked round-bottom flask (50 mL) equipped with a reflux condenser and a magnetic stirrer, 4,6-dichloropyrimidine (1 mmol) was dissolved in toluene (8 mL) and 1-hexadecylimidazole (2.2 mmol) was added under nitrogen. The mixture was stirred at reflux for 48 h, cooled, and the precipitate was isolated by filtration and then recrystallized from CH_2Cl_2/*n*-hexane to give $3a^{2+}\cdot 2Cl^-$. Yield: 56%. ^{1}H NMR (600 MHz, CD_2Cl_2, 20 °C): δ (ppm) 11.83 (s, 2H, imidazole-H), 10.66 (s, 1H, pyrimidine-H), 9.26 (s, 1H, pyrimidine-H), 8.85 (s, 2H, imidazole-H), 7.60 (s, 2H, imidazole-H), 4.48 (t, J = 7.2 Hz, 4H, NCH_2), 2.11−2.04 (m, 4H, NCH_2CH_2), 1.46−1.20 (m, 52H, $NC_2H_4(CH_2)_{13}$), 0.87 (t, J = 7.2 Hz, 6H, $NC_{15}H_{30}CH_3$). ^{13}C NMR (151 MHz, $CDCl_3$, 20 °C): δ (ppm) 159.57, 155.85, 136.98, 124.47, 119.90, 101.88, 51.49, 31.95, 30.02, 29.72, 29.70, 29.68, 29.59, 29.46, 29.38, 29.10, 26.35, 22.71, 14.13 (some of the signals for hexadecyl chains were overlapped). ESI-TOF-MS (positive, % intensity): m/z 331.3 (14), 331.8 (6), 697.6 (100), 698.6 (71). Calcd for $C_{42}H_{74}N_6^{2+}$ ($[M - 2Cl]^{2+}$), 662.60; $C_{42}H_{74}N_6Cl^+$ ($[M - Cl]^+$), 697.57. ESI-TOF-MS (negative, % intensity): m/z 767.5 (100), 768.5 (46). Calcd for $C_{42}H_{74}N_6Cl_3^-$ ($[M + Cl]^-$): 767.50. Elemental analysis: calcd (%) for $C_{42}H_{74}Cl_2N_6\cdot H_2O$, C 67.08, H 10.19, Cl 9.43, N 11.18, O 2.13; found C 67.11, H 10.44, Cl 9.43, N 11.25.

4,6-Bis(3-hexadecylimidazolium)pyrimidine Tetrafluoroborate, $3a^{2+}\cdot 2BF_4^-$. $3a^{2+}\cdot 2BF_4^-$ was prepared by the ion exchange of $3a^{2+}\cdot 2Cl^-$. $3a^{2+}\cdot 2Cl^-$ (0.19 mmol) was dissolved in CH_3OH (4 mL) and added to a solution of $LiBF_4$ (0.42 mmol) dissolved in water (2 mL) in a glass bottle. The mixture was stirred over 10 min until no further precipitate appeared. The precipitate was isolated by filtration and washed with EtOAc. Yield: 90%. ^{1}H NMR (600 MHz, $CDCl_3$, 20 °C): δ (ppm) 10.15 (s, 2H, imidazole-H), 9.26 (s, 1H, pyrimidine-H), 9.00 (s, 1H, pyrimidine-H), 8.53 (s, 2H, imidazole-H), 7.53 (s, 2H, imidazole-H), 4.38 (t, J = 7.2 Hz, 4H, NCH_2), 2.06−2.01 (m, 4H, NCH_2CH_2), 1.46−1.21 (m, 52H, $NC_2H_4(CH_2)_{13}$), 0.88 (t, J = 7.2 Hz, 6H, $NC_{15}H_{30}CH_3$). ^{13}C NMR (151 MHz, $CDCl_3$, 20 °C): δ (ppm) 159.29, 155.74, 135.85, 124.16, 119.87, 101.47, 51.46, 32.05, 29.85, 29.80, 29.74, 29.57, 29.49, 29.16, 26.39, 22.81, 14.24 (some of the signals for hexadecyl chains were overlapped). ESI-TOF-MS (positive, % intensity): m/z 331.3 (98), 331.8 (44), 749.6 (100), 750.6 (45). Calcd for $C_{42}H_{74}N_6^{2+}$ ($[M - 2BF_4]^{2+}$), 662.60; $C_{42}H_{74}N_6BF_4^+$ ($[M - BF_4]^+$), 749.60. ESI-TOF-MS (negative, % intensity): m/z 86.0 (19), 87.0 (100). Calcd for BF_4^- ($[0.5\ M - 0.5C_{42}H_{76}N_6]^-$): 87.00. UV/vis ($CH_2Cl_2$, λ_{max} [nm] (ε, 10^4 M^{-1} cm^{-1})): 269 (1.2). Elemental analysis: calcd (%) for $C_{42}H_{74}B_2F_8N_6$, C 60.29, H 8.91, B 2.58, F 18.17, N 10.04; found C 60.42, H 9.08, N 10.06 (for the species containing B, the exact value of F cannot be estimated).

4,6-Bis[3-(3,4,5-trihexadecyloxyphenyl)imidazolium]-pyrimidine Dichloride, $3b^{2+}\cdot 2Cl^-$. $3b^{2+}\cdot 2Cl^-$ was obtained by the reaction of 1-(3,4,5-trihexadecyloxyphenyl)imidazole, which was synthesized according to the literature,[6a,18] with 4,6-dichloropyrimidine.[13a] In a two-necked round-bottom flask (50 mL) equipped with a reflux condenser and a magnetic stirrer, 4,6-dichloropyrimidine (0.16 mmol) was dissolved in toluene (5 mL) and 1-(3,4,5-trihexadecyloxyphenyl)imidazole (0.34 mmol) was added under nitrogen. The mixture was stirred at reflux for 48 h, cooled, and the precipitate was isolated by filtration, chromatographed over flash silica gel column (eluent, MeOH/$CHCl_3$ = 1:10), and then recrystallized from $CHCl_3$/Et_2O to give $3b^{2+}\cdot 2Cl^-$. R_f = 0.29 (MeOH/$CHCl_3$ = 1:10). Yield: 16%. ^{1}H NMR (600 MHz, $CDCl_3$, 20 °C): δ (ppm) 12.01 (s, 2H, imidazole-H), 10.88 (s, 1H, pyrimidine-H), 9.28 (s, 1H, pyrimidine-H), 8.73 (s, 2H, imidazole-H), 8.29 (s, 2H, imidazole-H), 7.26 (s, 4H, Ar-H), 4.18−3.96 (m, 12H, OCH_2), 1.85−1.71 (m, 12H, OCH_2CH_2), 1.53−1.19 (m, 156H, $OC_2H_4(CH_2)_{13}$), 0.88 (t, J = 6.6 Hz, 18H, $OC_{15}H_{30}CH_3$). ^{13}C NMR (151 MHz, $CDCl_3$, 20 °C): δ (ppm) 155.58, 154.61, 140.16, 135.85, 129.29, 122.38, 120.01, 103.53, 101.30, 100.68, 73.89, 70.25, 32.04, 30.51, 30.46, 29.91, 29.90, 29.87, 29.84, 29.79, 29.68, 29.53, 29.48, 29.39, 26.36, 26.26, 26.19, 22.85, 14.26 (some of the signals for hexadecyl chains were overlapped). ESI-TOF-MS (positive, % intensity): m/z 1843.6 (100), 1844.6 (85). Calcd for $C_{118}H_{210}N_6O_6Cl^+$ ($[M - Cl]^+$): 1842.60. Elemental analysis: calcd (%) for $C_{118}H_{210}Cl_2N_6O_6\cdot 3H_2O$, C 73.28, H 11.26, Cl 3.67, N 4.35, O 7.45; found C 73.39, H 11.14, Cl 3.02, N 4.66.

General Procedures for Preparation of Ion Pairs Comprising Dicationic and Neutral Anion Receptors: $1b\cdot Cl^-$−$2a^{2+}\cdot Cl^-$ as a Representative. A solution of **1b** and $2a^{2+}\cdot 2Cl^-$ with an equivalent molar ratio in CH_2Cl_2 was evaporated under reduced pressure. The dissolution−evaporation process was repeated at least three times to yield $1b\cdot Cl^-$−$2a^{2+}\cdot Cl^-$ as an orange solid. ^{1}H NMR (600 MHz, CD_2Cl_2, 20 °C. Partial complexation was observed under the condition, although [1 + 1]-type receptor−anion complexes were constructed in bulk state. The precise integrations of pyrrole NH were not determined because of the broad signals in the anion-free state.): δ (ppm) 11.98 (br, anion-binding pyrrole-NH), 11.37 (s, 2H, imidazole-H), 9.96 (br, anion-free pyrrole-NH), 8.79 (s, 1H, Ar-H), 8.47 (br, 1H, bridging CH), 8.41 (s, 2H, imidazole-H), 8.08 (br, 4H, Ar-H), 7.73 (d, J = 8.4 Hz, 2H, Ar-H), 7.53 (t, J = 7.8 Hz, 1H, Ar-H), 7.44 (br, 4H, Ar-H), 7.34 (br, 2H, Ar-H), 7.20 (s, 2H, imidazole-H), 7.03 (br, 2H, pyrrole-H), 6.69 (br, 2H, pyrrole-H), 4.19 (t, J = 6.6 Hz, 4H, NCH_2), 1.99−1.94 (m, 4H, NCH_2CH_2), 1.39−1.21 (m, 52H, $NC_2H_4(CH_2)_{13}$), 0.88 (t, J = 7.2 Hz, 6H, $NC_{15}H_{30}CH_3$). Elemental analysis: calcd (%) for $C_{67}H_{93}BCl_2F_2N_6O_2$, C 70.95, H 8.26, B 0.95, Cl 6.25, F 3.35, N 7.41, O 2.82; found C 70.40, H 8.51, N 7.03 (for the species containing B and F, the exact values of O and Cl cannot be estimated).

$1c\cdot Cl^-$−$2a^{2+}\cdot Cl^-$. ^{1}H NMR (600 MHz, CD_2Cl_2, 20 °C. Partial complexation was observed under the condition, although [1 + 1]-type receptor−anion complexes were constructed in bulk state. The precise integrations of pyrrole NH were not determined because of the broad signals in the anion-free state.): δ (ppm) 11.79 (br, anion-binding pyrrole-NH), 11.22 (s, 2H, imidazole-H), 9.72 (br, anion-free pyrrole-NH), 8.69 (s, 1H, Ar-H), 8.45 (s, 2H, imidazole-H), 8.36 (br, 1H, bridging CH), 7.66 (d, J = 7.8 Hz, 2H, Ar-H), 7.48 (t, J = 7.2 Hz, 1H, Ar-H), 7.22 (s, 4H, Ar-H), 7.20 (s, 2H, imidazole-H), 6.93 (br, 1.5H, receptor−anion-complex pyrrole-H), 6.86 (br, 0.5H, anion-free-receptor pyrrole-H), 6.67 (br, 0.5H, anion-free-receptor pyrrole-H), 6.59 (br, 1.5H, receptor−anion-complex pyrrole-H), 4.23−4.19 (m, 12H, OCH_2), 3.97 (t, J = 6.6 Hz, 4H, NCH_2), 1.99−1.94 (m, 4H, NCH_2CH_2), 1.86−1.73 (m, 12H, OCH_2CH_2), 1.56−1.20 (m, 208H, $OC_2H_4(CH_2)_{13}$ and $NC_2H_4(CH_2)_{13}$), 0.88 (t, J = 6.6 Hz, 24H, $OC_{15}H_{30}CH_3$ + $NC_{15}H_{30}CH_3$). Elemental analysis: calcd (%) for $C_{163}H_{285}BCl_2F_2N_6O_8$, C 75.98, H 11.15, B 0.42, Cl 2.75, F 1.47, N 3.26, O 4.97; found C 75.68, H 11.41, N 3.24 (for the species containing B and F, the exact values of O and Cl cannot be estimated).

$1b\cdot Cl^-$−$3a^{2+}\cdot Cl^-$. ^{1}H NMR (600 MHz, CD_2Cl_2, 20 °C. Partial complexation was observed under the condition, although [1 + 1]-type receptor−anion complexes were constructed in bulk state. The precise integrations of pyrrole NH were not determined because of the broad signals in the anion-free state.): δ (ppm) 11.98 (br, anion-binding pyrrole-NH), 11.27 (s, 2H, imidazole-H), 10.32 (s, 1H, pyrimidine-H), 9.83 (br, anion-free pyrrole-NH), 8.87 (s, 1H, pyrimidine-H), 8.54 (s, 2H, imidazole-H), 8.37 (br, 1H, bridging CH), 8.10 (br, 4H, Ar-H), 7.46 (t, J = 7.2 Hz, 4H, Ar-H), 7.34 (br, 2H, Ar-H), 7.21 (s, 2H, imidazole-H), 7.14 (br, 2H, pyrrole-H), 6.74 (br, 2H, pyrrole-H), 4.18 (t, J = 7.2 Hz, 4H, NCH_2), 1.99−1.94 (m, 4H, NCH_2CH_2), 1.38−1.23 (m, 52H, $NC_2H_4(CH_2)_{13}$), 0.88 (t, J = 6.6 Hz, 6H, $NC_{15}H_{30}CH_3$). Elemental analysis: calcd (%) for $C_{65}H_{91}BCl_2F_2N_8O_2$: C 68.71, H 8.07, B 0.95, Cl 6.24, F 3.34, N 9.86, O 2.82; found C 68.03, H 8.14, N 9.64 (for the species containing B and F, the exact values of O and Cl cannot be estimated).

$1c\cdot Cl^-$−$3a^{2+}\cdot Cl^-$. ^{1}H NMR (600 MHz, CD_2Cl_2, 20 °C. Partial complexation was observed under the condition, although [1 + 1]-type receptor−anion complexes were constructed in bulk state. The precise integrations of pyrrole NH were not determined because of the broad signals in the anion-free state.): δ (ppm) 11.79 (br, anion-binding pyrrole-NH), 11.11 (s, 2H, imidazole-H), 10.21 (s, 1H, pyrimidine-

dx.doi.org/10.1021/ja4071333 | J. Am. Chem. Soc. 2013, 135, 14797−14805

H), 9.56 (br, anion-free pyrrole-NH), 9.04 (s, 1H, pyrimidine-H), 8.65 (br, 1H, bridging CH), 8.60 (s, 2H, imidazole-H), 7.26 (s, 4H, Ar-H), 7.23 (s, 2H, imidazole-H), 6.99 (br, 1.2H, receptor−anion-complex pyrrole-H), 6.97 (br, 0.8H, anion-free-receptor pyrrole-H), 6.65 (br, 2H, pyrrole-H), 4.27−4.21 (m, 12H, OCH_2), 3.93 (t, J = 6.0 Hz, 4H, NCH_2), 2.04−1.97 (m, 4H, NCH_2CH_2), 1.86−1.71 (m, 12H, OCH_2CH_2), 1.50−1.20 (m, 208H, $OC_2H_4(CH_2)_{13}$ and $NC_2H_4(CH_2)_{13}$), 0.88 (t, J = 7.2 Hz, 24H, $OC_{15}H_{30}CH_3$ and $NC_{15}H_{30}CH_3$). Elemental analysis: calcd (%) for $C_{161}H_{283}BCl_2F_2N_8O_8$, C 74.99, H 11.06, B 0.42, Cl 2.75, F 1.47, N 4.35, O 4.96; found C 75.02, H 11.32, N 4.31 (for the species containing B and F, the exact values of O and Cl cannot be estimated).

1b·Cl⁻−3b²⁺·Cl⁻. ^{1}H NMR (600 MHz, CD_2Cl_2, 20 °C. Partial complexation was observed under the condition, although [1 + 1]-type receptor−anion complexes were constructed in bulk state. The precise integrations of pyrrole NH were not determined because of the broad signals in the anion-free state.): δ (ppm) 11.84 (br, anion-binding pyrrole-NH), 11.61 (s, 2H, imidazole-H), 10.54 (s, 1H, pyrimidine-H), 9.87 (br, anion-free pyrrole-NH), 8.83 (s, 1H, pyrimidine-H), 8.42 (br, 1H, bridging CH), 8.31 (s, 2H, imidazole-H), 8.00 (br, 4H, Ar-H), 7.70 (s, 2H, imidazole-H), 7.46 (s, 4H, Ar-H), 7.26 (br, 4H, Ar-H), 7.16 (br, 2H, Ar-H), 7.07 (br, 1.2H, receptor−anion-complex pyrrole-H), 7.04 (br, 0.8H, anion-free-receptor pyrrole-H), 6.75 (br, 0.8H, anion-free-receptor pyrrole-H), 6.64 (br, 1.2H, receptor−anion-complex pyrrole-H), 4.14−4.00 (m, 12H, OCH_2), 1.87−1.75 (m, 12H, OCH_2CH_2), 1.43−1.18 (m, 156H, $OC_2H_4(CH_2)_{13}$), 0.88 (t, J = 7.2 Hz, 18H, $OC_{15}H_{30}CH_3$). Elemental analysis: calcd (%) for $C_{141}H_{227}BCl_2F_2N_8O_8$, C 74.21, H 10.03, B 0.47, Cl 3.11, F 1.67, N 4.91, O 5.61; found C 74.46, H 10.18, N 4.70 (for the species containing B and F, the exact values of O and Cl cannot be estimated).

1c·Cl⁻−3b²⁺·Cl⁻. ^{1}H NMR (600 MHz, CD_2Cl_2, 35 °C due to the less solubility at 20 °C to partially give precipitates. Partial complexation was observed under the condition, although [1 + 1]-type receptor−anion complexes were constructed in bulk state. The precise integrations of pyrrole NH were not determined because of the broad signals in the anion-free state.): δ (ppm) 11.80 (br, anion-binding pyrrole-NH), 11.68 (s, 2H, imidazole-H), 10.51 (s, 1H, pyrimidine-H), 9.66 (br, anion-free pyrrole-NH), 9.07 (s, 1H, pyrimidine-H), 8.69 (br, 1H, bridging CH), 8.33 (s, 2H, imidazole-H), 7.62 (s, 2H, imidazole-H), 7.17 (s, 4H, Ar-H), 7.12 (s, 4H, Ar-H), 6.99 (br, 1.8H, receptor−anion-complex pyrrole-H), 6.98 (br, 0.2H, anion-free-receptor pyrrole-H), 6.62 (br, 1.8H, receptor−anion-complex pyrrole-H), 6.61 (br, 0.2H, anion-free-receptor pyrrole-H), 4.20−4.09 (m, 12H, OCH_2), 4.03−3.88 (m, 12H, OCH_2), 1.90−1.69 (m, 24H, OCH_2CH_2), 1.50−1.24 (m, 312H, $OC_2H_4(CH_2)_{13}$), 0.88 (t, J = 6.6 Hz, 36H, $OC_{15}H_{30}CH_3$). Elemental analysis: calcd (%) for $C_{237}H_{419}BCl_2F_2N_8O_{14}$, C 76.42, H 11.34, B 0.29, Cl 1.90, F 1.02, N 3.01, O 6.01; found C 76.54, H 11.57, N 3.05 (for the species containing B and F, the exact values of O and Cl cannot be estimated).

Ab Initio and Semiempirical Calculations. DFT calculations and semiempirical calculations at the AM1 level were carried out by using the Gaussian 03 program.[14] Unless otherwise noted, the calculation was performed in the gas phase. Mapping of electrostatic potentials and graphical outputs were done using MOLEKEL, version 5.4.[19]

Estimation of Binding Constants. K_a values for 1:1 binding were estimated by least-squares curve-fitting for the titration plots (concentrations of added guest species (x) vs spectral changes (y)) according to the following equation:

$$y = y_0 \frac{(K_a x + K_a a + 1) - \sqrt{(K_a x + K_a a + 1)^2 - 4K_a a x}}{2K_a a}$$

wherein a is an initial concentration of host species and y_0 is a parameter to be estimated by fitting.[20]

Scanning Electron Microscopy (SEM). SEM images were obtained with a HITACHI S-4800 scanning electron microscope at acceleration voltages of 10 kV using a silicon (100) substrate. A platinum coating was applied using a HITACHI E-1030 ion sputter.

Differential Scanning Calorimetry (DSC). The phase transitions were measured on a differential scanning calorimetry (Perkin-Elmer Diamond DSC).

Polarized Optical Microscopy (POM). The textures were observed by using a polarization microscope (Nikon ECLIPSE E600 POL), equipped with a heating plate (Mettler FP-82 HT hot stage) controlled by a thermoregulator (Mettler FP-90 central processor).

Synchrotron X-ray Diffraction (XRD) Analysis. High-resolution XRD analyses were carried out using a synchrotron radiation X-ray beam with a wavelength of 1.00 Å on BL40B2 at SPring-8 (Hyogo, Japan). A large Debye−Scherrer camera with camera lengths of 540.18 mm for **2a**²⁺·2Cl⁻ and **1b**·Cl⁻-**2a**²⁺·Cl⁻ and 546.28 mm for **3a**²⁺·2Cl⁻, **3b**²⁺·Cl⁻, **1c**·Cl⁻-**2a**²⁺·Cl⁻, **1c**·Cl⁻-**3a**²⁺·Cl⁻, and **1c**·Cl⁻-**3b**²⁺·Cl⁻ was used with an imaging plate as a detector. The sample was sealed in a quartz capillary where the diffraction pattern was obtained with a 0.01° step in 2θ under the exposure time of 10 or 30 s depending on the intensity of diffraction peaks.

Flash-Photolysis Time-Resolved Microwave Conductivity (FP-TRMC). The charge carrier mobility was measured by FP-TRMC technique. **1c**·Cl⁻−**2a**²⁺·Cl⁻ and **1c**·Cl⁻−**3a**²⁺·Cl⁻ were mounted on a quartz plate, once heated up to the isotropic state, and then cooled to room temperature, affording thin film samples, respectively. Charge carriers were photochemically generated using a third harmonic generation (λ = 355 nm) of a Spectra Physics model INDI-HG Nd:YAG laser with a pulse duration of 5−8 ns. The photon density of a 355 nm pulse was 0.9×10^{16} photons cm^{-2}. The microwave frequency and power were set at ∼9.1 GHz and 3 mW, respectively. The TRMC signal, picked up by a diode (rise time of <1 ns), was monitored by a Tektronics model TDS3052B digital oscilloscope. The observed conductivities were normalized, given by a photocarrier generation yield (ϕ) multiplied by sum of the charge carrier mobilities ($\sum\mu$), according to the equation, $\phi\sum\mu = [(1/e)AI_0F_{light}](\Delta P_r/P_r)$, where, e, A, I_0, F_{light}, P_r, and ΔP_r are unit charge of a single electron, sensitivity factor (S^{-1} cm), incident photon density of the excitation laser (photon cm^{-2}), correction (or filling) factor (cm^{-1}), and reflected microwave power and its change, respectively. The ϕ values were determined by direct current integration method. An interdigitated comb-type gold electrode with 5 μm gaps, 40 nm height, and 2 mm width was fabricated by a lithographic process on a glass substrate. Samples were fabricated by mounting **1c**·Cl⁻−**3a**²⁺·Cl⁻ and **1c**·Cl⁻−**3b**²⁺·Cl⁻ on the electrodes followed by a heating−cooling process, respectively. The samples were exposed to a 355 nm pulse with 0.9×10^{16} photons cm^{-2}. Current transients were monitored by a Tektronix model TDS3052B digital oscilloscope equipped with a 10 kΩ termination resistance. The applied voltage was controlled by an Advantest Corp. model R8252 digital electrometer. All the experiments were carried out at room temperature.

■ ASSOCIATED CONTENT

Ⓢ Supporting Information

DSC profiles, POM images, and XRD patterns. This material is available free of charge via the Internet at http://pubs.acs.org.

■ AUTHOR INFORMATION

Corresponding Authors

seki@chem.eng.osaka-u.ac.jp

maedahir@ph.ritsumei.ac.jp

Present Address

[∞]School of Chemistry and Chemical Engineering, Jiangsu Normal University, Xuzhou 221116, China

Notes

The authors declare no competing financial interest.

■ ACKNOWLEDGMENTS

This work was supported by Grant-in-Aid for Young Scientists (A) (Grant No. 23685032) from the MEXT and Ritsumeikan R-GIRO project (2008−2013). We thank Dr. Takashi

Nakanishi, NIMS, for SEM measurements, Dr. Noboru Ohta, JASRI/SPring-8, for synchrotron radiation XRD measurements (BL40B2 at SPring-8), Prof. Tomonori Hanasaki, Ritsumeikan University, for DSC and POM measurements, RIKEN Integrated Cluster of Clusters (RICC) for the computer resources, and Prof. Hitoshi Tamiaki, Ritsumeikan University, for various measurements. T.S. and Y.B. also thank JSPS for a Research Fellowship for Young Scientists.

REFERENCES

(1) Selected reviews on ionic liquid crystals: (a) Binnemans, K. *Chem. Rev.* **2005**, *105*, 4148−4204. (b) Kato, T.; Yasuda, T.; Kamikawa, Y.; Yoshio, M. *Chem. Commun.* **2009**, 729−739.

(2) Selected reviews on hybrid materials comprising charged species: (a) Faul, C. F. J.; Antonietti, M. *Adv. Mater.* **2003**, *15*, 673−683. (b) Bideau, J. L.; Viau, L.; Vioux, A. *Chem. Soc. Rev.* **2011**, *40*, 907−925. (c) Wang, C.; Wang, Z.; Zhang, X. *Acc. Chem. Res.* **2012**, *45*, 608−618.

(3) Selected reports of stacking planar cations: (a) Laursen, B. W.; Krebs, F. C.; Nielsen, M. F.; Bechgaard, K.; Christensen, J. B.; Harrit, N. *J. Am. Chem. Soc.* **1998**, *120*, 12255−12263. (b) Yuen, M.-Y.; Roy, V. A. L.; Lu, W.; Kui, S. C. F.; Tong, G. S. M.; So, M.-H.; Chui, S. S.-Y.; Muccini, M.; Ning, J. Q.; Xu, S. J.; Che, C.-M. *Angew. Chem., Int. Ed.* **2008**, *47*, 9895−9899. (c) Wu, D.; Pisula, W.; Enkelmann, V.; Feng, X.; Müllen, K. *J. Am. Chem. Soc.* **2009**, *131*, 9620−9621. (d) Fortage, J.; Tuyèras, F.; Ochsenbein, P.; Puntoriero, F.; Nastasi, F.; Campagna, S.; Griveau, S.; Bedioui, F.; Ciofini, I.; Lainé, P. P. *Chem.—Eur. J.* **2010**, *16*, 11047−11063.

(4) Selected books on anion binding: (a) *Supramolecular Chemistry of Anion*; Bianchi, A., Bowman-James, K., García-España, E., Eds.; Wiley-VCH: New York, 1997. (b) *Fundamentals and Applications of Anion Separation*; Singh, R. P., Moyer, B. A., Eds.; Kluwer Academic/Plenum Publishers: New York, 2004. (c) *Anion Sensing*; Stibor, I., Ed.; Topics in Current Chemistry, Vol. *255*; Springer-Verlag: Berlin, 2005; pp 1−238. (d) Sessler, J. L.; Gale, P. A.; Cho, W.-S. *Anion Receptor Chemistry*; Royal Society of Chemistry: Cambridge, U.K., 2006. (e) *Recognition of Anions*; Vilar, R., Ed.; *Structure and Bonding*, Vol. *129*; Springer-Verlag: Berlin, 2008; pp 1−252. (f) *Anion Recognition in Supramolecular Chemistry*; Gale, P. A., Dehaen, W., Eds.; Topics in Heterocyclic Chemistry, Vol. *24*; Springer-Verlag: Berlin, 2010; pp 1−370. (g) *Anion Coordination Chemistry*; Bowman-James, K.; Bianchi, A.; García-España, E., Eds.; Wiley-VCH: New York, 2011.

(5) Selected reports: (a) Li, Y.; Flood, A. H. *Angew. Chem., Int. Ed.* **2008**, *47*, 2649−2652. (b) Juwarker, H.; Lendhardt, J. M.; Pham, D. M.; Craig, S. L. *Angew. Chem., Int. Ed.* **2008**, *47*, 3740−3743. (c) Li, Y.; Flood, A. H. *J. Am. Chem. Soc.* **2008**, *130*, 12111−12122. (d) Hua, Y.; Flood, A. H. *J. Am. Chem. Soc.* **2010**, *132*, 12838−12840. (e) Lee, S.; Chen, C.-H.; Flood, A. H. *Nature Chem.* **2013**, *5*, 704−710.

(6) (a) Maeda, H.; Haketa, Y.; Nakanishi, T. *J. Am. Chem. Soc.* **2007**, *129*, 13661−13674. (b) Maeda, H.; Terasaki, M.; Haketa, Y.; Mihashi, Y.; Kusunose, Y. *Org. Biomol. Chem.* **2008**, *6*, 433−436. (c) Maeda, H.; Terashima, Y.; Haketa, Y.; Asano, A.; Honsho, Y.; Seki, S.; Shimizu, M.; Mukai, H.; Ohta, K. *Chem. Commun.* **2010**, *46*, 4559−4561. (d) Haketa, Y.; Bando, Y.; Takaishi, K.; Uchiyama, M.; Muranaka, A.; Naito, M.; Shibaguchi, H.; Kawai, T.; Maeda, H. *Angew. Chem., Int. Ed.* **2012**, *51*, 7967−7971.

(7) A recent review on materials comprising planar charged species: Dong, B.; Maeda, H. *Chem. Commun.* **2013**, *49*, 4085−4099.

(8) Charge-by-charge assemblies: (a) Haketa, Y.; Sasaki, S.; Ohta, N.; Masunaga, H.; Ogawa, H.; Mizuno, N.; Araoka, F.; Takezoe, H.; Maeda, H. *Angew. Chem., Int. Ed.* **2010**, *49*, 10079−10083. (b) Maeda, H.; Naritani, K.; Honsho, Y.; Seki, S. *J. Am. Chem. Soc.* **2011**, *133*, 8896−8899. (c) Dong, B.; Terashima, Y.; Haketa, Y.; Maeda, H. *Chem.—Eur. J.* **2012**, *18*, 3460−3463. (d) Bando, Y.; Sakamoto, S.; Yamada, I.; Haketa, Y.; Maeda, H. *Chem. Commun.* **2012**, *48*, 2301−2303.

(9) Charge-segregated assemblies: (a) Haketa, Y.; Honsho, Y.; Seki, S.; Maeda, H. *Chem.—Eur. J.* **2012**, *18*, 7016−7020. (b) Dong, B.; Sakurai, T.; Honsho, Y.; Seki, S.; Maeda, H. *J. Am. Chem. Soc.* **2013**, *135*, 1284−1287.

(10) (a) Laursen, B. W.; Krebs, F. C. *Angew. Chem., Int. Ed.* **2000**, *39*, 3432−3434. (b) Laursen, B. W.; Krebs, F. C. *Chem.—Eur. J.* **2001**, *7*, 1773−1783.

(11) Recent reviews: (a) Yoon, J.; Kim, S. K.; Singh, N. J.; Kim, K. S. *Chem. Soc. Rev.* **2006**, *35*, 355−360. (b) Xu, Z.; Kim, S. K.; Yoon, J. *Chem. Soc. Rev.* **2010**, *39*, 1457−1466.

(12) Selected reports of single-crystal X-ray structures: (a) Kim, H. N.; Lim, J.; Lee, H. N.; Ryu, J.-W.; Kim, M. J.; Lee, J.; Lee, D.-U.; Kim, Y.; Kim, S.-J.; Lee, K. D.; Lee, H.-S.; Yoon, J. *Org. Lett.* **2011**, *13*, 1314−1317. (b) Zuo, W.; Braunstein, P. *Organometallics* **2012**, *31*, 2606−2615.

(13) (a) Sato, K.; Takeuchi, S.; Arai, S.; Yamaguchi, M.; Yamagishi, T. *Heterocycles* **2007**, *73*, 209−215. (b) Rit, A.; Pape, T.; Hahn, F. E. *J. Am. Chem. Soc.* **2010**, *132*, 4572−4573.

(14) For optimized structures of neutral anion receptors (refs 6a, 6b, and 8a) and positively charged anion receptors along with receptor−anion complexes: Frisch, M. J.; Trucks, G. W.; Schlegel, H. B.; Scuseria, G. E.; Robb, M. A.; Cheeseman, J. R.; Montgomery, J. A., Jr.; Vreven, T.; Kudin, K. N.; Burant, J. C.; Millam, J. M.; Iyengar, S. S.; Tomasi, J.; Barone, V.; Mennucci, B.; Cossi, M.; Scalmani, G.; Rega, N.; Petersson, G. A.; Nakatsuji, H.; Hada, M.; Ehara, M.; Toyota, K.; Fukuda, R.; Hasegawa, J.; Ishida, M.; Nakajima, T.; Honda, Y.; Kitao, O.; Nakai, H.; Klene, M.; Li, X.; Knox, J. E.; Hratchian, H. P.; Cross, J. B.; Adamo, C.; Jaramillo, J.; Gomperts, R.; Stratmann, R. E.; Yazyev, O.; Austin, A. J.; Cammi, R.; Pomelli, C.; Ochterski, J. W.; Ayala, P. Y.; Morokuma, K.; Voth, G. A.; Salvador, P.; Dannenberg, J. J.; Zakrzewski, V. G.; Dapprich, S.; Daniels, A. D.; Strain, M. C.; Farkas, O.; Malick, D. K.; Rabuck, A. D.; Raghavachari, K.; Foresman, J. B.; Ortiz, J. V.; Cui, Q.; Baboul, A. G.; Clifford, S.; Cioslowski, J.; Stefanov, B. B.; Liu, G.; Liashenko, A.; Piskorz, P.; Komaromi, I.; Martin, R. L.; Fox, D. J.; Keith, T.; Al-Laham, M. A.; Peng, C. Y.; Nanayakkara, A.; Challacombe, M.; Gill, P. M. W.; Johnson, B.; Chen, W.; Wong, M. W.; Gonzalez, C.; Pople, J. A. *Gaussian 03*, revision C.01; Gaussian, Inc.: Wallingford, CT, 2004.

(15) (a) Saeki, A.; Seki, S.; Sunagawa, T.; Ushida, K.; Tagawa, S. *Philos. Mag.* **2006**, *86*, 1261−1276. (b) Saeki, A.; Koizumi, Y.; Aida, T.; Seki, S. *Acc. Chem. Res.* **2012**, *45*, 1193−1202. (c) Yasutani, Y.; Saeki, A.; Fukumatsu, T.; Koizumi, Y.; Seki, S. *Chem. Lett.* **2013**, *42*, 19−21.

(16) Atoji, M.; Richardson, J. W.; Rundle, R. E. *J. Am. Chem. Soc.* **1957**, *79*, 3017−3020.

(17) Colonna, M.; Berti, C.; Binassi, E.; Fiorini, M.; Sullalti, S.; Acquasanta, F.; Vannini, M.; Gioia, D. D.; Aloisio, I.; Karanam, S.; Brunelle, D. *React. Funct. Polym.* **2012**, *77*, 133−141.

(18) Wang, L.; Woods, K. W.; Li, Q.; Barr, K. J.; McCroskey, R. W.; Hannick, S. M.; Gherke, L.; Credo, R. B.; Hui, Y.-H.; Marsh, K.; Warner, R.; Lee, J. Y.; Zielinski-Mozng, N.; Frost, D.; Rosenberg, S. H.; Sham, H. L. *J. Med. Chem.* **2002**, *45*, 1697−1711.

(19) Varetto, U. *MOLEKEL*, version 5.4; Swiss National Supercomputing Centre: Manno, Switzerland.

(20) Connors, K. A. *Binding Constants*; John Wiley & Sons: New York, 1987.